

Article

First-Principle Study of $\text{Ca}_3\text{Y}_2\text{Ge}_3\text{O}_{12}$ Garnet: Dynamical, Elastic Properties and Stability under Pressure

Alfonso Muñoz *  and Plácida Rodríguez-Hernández

Departamento de Física, Instituto de Materiales y Nanotecnología, Malta Consolider Team, Universidad de La Laguna, 38200 La Laguna, Tenerife, Spain

* Correspondence: amunoz@ull.edu.es; Tel.: +34-922-318-275

Abstract: We present here an ab initio study under the framework of the Density Functional Theory of the $\text{Ca}_3\text{Y}_2\text{Ge}_3\text{O}_{12}$ garnet. Our study focuses on the analysis of the structural, electronic, dynamic, and elastic properties of this material under hydrostatic pressure. We report information regarding the equation of state, the compressibility, and the structural evolution of this compound. The dynamical properties and the evolution under pressure of infrared, silent, and Raman frequencies and their pressure coefficients are also presented. The dependence on the pressure of the elastic constants and the mechanical and elastic properties are analyzed. From our results, we conclude that this garnet becomes mechanically unstable at 45.7 GPa; moreover, we also find evidence of soft phonons at 34.4 GPa, showing the dynamical instability of this compound above this pressure.

Keywords: ab initio; garnet; equation of state; elasticity; phonons; Raman

1. Introduction

The study of garnet minerals under high pressure is an essential topic in Earth Sciences; garnets are among the major components of Earth's deep interior. The physical properties of these materials at extreme conditions have an important effect on the dynamics of the mantle transition zone [1].

In technological applications, garnets are potential candidates for many devices. Their excellent thermal conductivity, hardness, mechanical and chemical stability, and high optical transparency suggest that these materials can be used as laser materials. Doping garnets with Rare Earth (RE^{3+}) elements allows the use of their great luminescence properties. For example, YAG, a $\text{Y}_3\text{Al}_5\text{O}_3$ garnet, used as a solid-state laser doped with Nd, is well-known in medical and commercial applications [2]. Under pressure, these garnets can be employed as sensors for high-pressure experiments [3,4], and can also be used with adequate doping as scintillators or light-emitting diodes [5]. Recently, a $\text{Ca}_3\text{Y}_2\text{Ge}_3\text{O}_{12}$ garnet doped with Cr^{+3} was studied as a near-infrared LED combined with a 455 nm LED chip [6]. In addition, the near-infrared phosphor $\text{Ca}_3\text{Y}_2\text{Ge}_3\text{O}_{12}:\text{Cr}^{+3}$ garnet has been synthesized, showing a broadband NIR emission of 700–1100 nm, peaking around 800 nm [7].

The oxide garnets have the general formula $\text{A}_3\text{B}_2\text{C}_3\text{O}_{12}$, where A denotes the dodecahedral, B the octahedral, and C the tetrahedral sites with different coordination. They usually crystallize in the body-centered cubic (bcc) structure ($Ia\bar{3}d$ space group), with a unit cell of 160 atoms and a primitive cell of 80 atoms. In our case, Ca atoms (A) occupy the 24 *c* positions with coordination 8, Y atoms (B) occupy the 16 *a* positions with coordination 6 and octahedral point symmetry (C_{3i}), and Ge atoms (C) occupy the 24 *d* positions with coordination 4 and tetrahedral point symmetry (S_4). Finally, the O atoms occupy the 96 *h* positions (Figure 1).



Citation: Muñoz, A.; Rodríguez-Hernández, P. First-Principle Study of $\text{Ca}_3\text{Y}_2\text{Ge}_3\text{O}_{12}$ Garnet: Dynamical, Elastic Properties and Stability under Pressure. *Crystals* **2023**, *13*, 29. <https://doi.org/10.3390/cryst13010029>

Academic Editor: Claudio Cazorla

Received: 5 December 2022

Revised: 19 December 2022

Accepted: 21 December 2022

Published: 24 December 2022



Copyright: © 2022 by the authors. Licensee MDPI, Basel, Switzerland. This article is an open access article distributed under the terms and conditions of the Creative Commons Attribution (CC BY) license (<https://creativecommons.org/licenses/by/4.0/>).

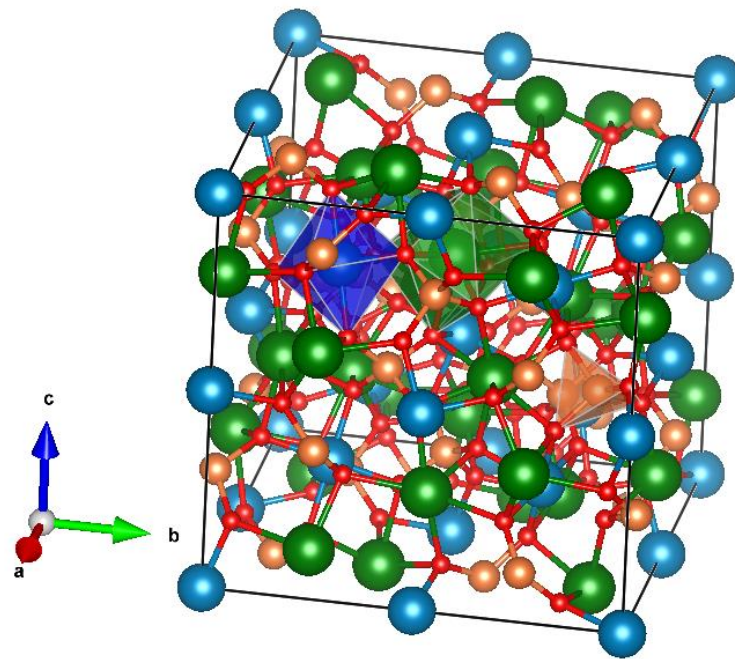


Figure 1. The conventional unit cell with polyhedral units CaO_8 (green), YO_6 (blue), and GeO_4 (orange).

Due to the large number of atoms in the unit cell and hence the complexity of the simulation, few *ab initio* studies of the structural, electronic, dynamical, or mechanical properties both at room and high pressures are available for garnets [8,9].

In the last decades, the use of Density Functional Theory (DFT) simulations of material under high pressure has become a very well-established technique. The quality and precision of these studies make possible the prediction of many properties of materials under extreme conditions, providing information on the stability of these compounds.

The application of pressure allows modifications of the bonds and interatomic distances of material and, therefore, changes in their elastic and vibrational properties. On the other hand, the optical properties of Re^{3+} doped oxides garnets are affected by changes in the host structure due to the reduction in interatomic distances and possible coordination changes. Thus, it is worth studying garnets' structural and electronic properties under pressure to help understand their luminescence properties and improve their practical applications. A study of this garnet under pressure is required to explore potential applications of the $\text{Ca}_3\text{Y}_2\text{Ge}_3\text{O}_{12}$ garnet, for example, as a pressure optical sensor. The knowledge of its mechanical properties under pressure is also essential in geological studies due to the abundance of this mineral phase in the upper mantle and Earth's transition zone [10].

Since it is important to study how the properties of garnets evolve under high pressure, in this work, we report an extensive first-principle study of the electronic, structural, dynamic, and elastic properties of the $\text{Ca}_3\text{Y}_2\text{Ge}_3\text{O}_{12}$ garnet under pressure. To the best of our knowledge, there are no reported *ab initio* studies of this compound under high pressure. We hope the information provided in this work will stimulate further experimental studies on this garnet.

2. Simulation Details

Ab initio total energy simulations at zero temperature were performed in the framework of the Density Functional Theory, DFT, with the plane-wave method and the pseudopotential theory implemented in the Vienna *ab initio* simulations package [11,12]. The Projector Augmented-Wave (PAW) [13] pseudopotentials provided in this package were employed to take into account the full nodal character of the all-electron charge density in the core region. For the Ca atoms, 8 valence electrons ($3p^64s^2$) were included, for Y atoms

11 valence electrons ($4s^2 4p^6 5s^2 4d^1$), and for Ge atoms 14 valence electrons ($3d^{10} 4s^2 4p^2$), whereas for O atoms 6 valence electrons ($2s^2 2p^4$) were used. The basis set included plane waves up to a cut-off energy of 520 eV in order to achieve highly converged results. The exchange–correlation energy was described with the generalized gradient approximation, GGA, using the PBEsol functional [14]. The integrations over the Brillouin zone, BZ, were performed with a $4 \times 4 \times 4$ Monkorts-Pack grid [15] k-points sampling to obtain accurate converged energies and forces. At a set of selected volumes, the structure was fully optimized to obtain its equilibrium configuration through the calculations of forces and stress tensors. The convergence criteria were to achieve forces smaller than $0.004 \text{ eV}/\text{\AA}$ and deviations of stress tensor diagonal lower than 0.1 GPa. The data set of volume (V) and energy (E) obtained as result of our simulations was fitted with a standard equation of state, EOS, to determine the bulk modulus and its pressure derivative.

Lattice-dynamic calculations of the phonon modes were carried out at the zone center (Γ point) of the BZ with the direct force-constant approach [16]. These calculations provide the frequency of the normal modes, their symmetry, and their polarization vectors. This allowed to identify the irreducible representations and the character of the phonon modes at the Γ -point. The study of the dynamical stability was performed through the phonon density of state and the phonon dispersion calculated using a $2 \times 2 \times 2$ supercell.

The mechanical and elastic properties were studied by obtaining the elastic constants with the strain–stress method implemented in the VASP code following Le Page method [17].

3. Results and Discussion

3.1. Structural Properties under Pressure

From our ab initio simulations, the obtained unit cell volume at zero pressure is 2095.5 \AA^3 with a lattice constant of $a_0 = 12.7966 \text{ \AA}$, and the O 96 *h* positions are defined by $x = 0.9646$, $y = 0.0573$, and $z = 0.1610$ (experiment $a = 12.8059 \text{ \AA}$, O 96*h* positions: 0.9637, 0.0567, and 0.1609) [18]. Our results are in excellent agreement with the available experimental data, and they differ by less than 0.3%. The Ca, Y, and Ge atoms occupy fixed Wyckoff positions already described in a previous section. In Table 1, we report the calculated structural parameter, the bulk modulus, and its pressure derivative. The bulk modulus, $B_0 = 111.24 \text{ GPa}$, with a pressure derivative B_0' of 4.75, was obtained from the theoretical energy and volume data using a Birch–Murnaghan EOS [19]. This bulk modulus is smaller than those of most silicate garnets (between 150 and 190 GPa) [10,20], due to the smaller ionic radius of Ca.

Table 1. The lattice constant, a_0 , the volume, V_0 , at zero pressure, and the bulk modulus, B_0 , and its pressure derivative B_0' .

	a_0 (Å)	V_0 (Å ³)	B_0 (GPa)	B_0'
This work	12.7966	2095.5	111.24	4.75
Experiment ¹	12.8059	2100.05	-	-

¹ Reference [18].

The volume versus pressure evolution of the $\text{Ca}_3\text{Y}_2\text{Ge}_3\text{O}_{12}$ garnet is presented in Figure 2, and the inset shows the lattice constant evolution. The linear axial compressibility, $k_a = 0.255 \times 10^{-3} \text{ GPa}^{-1}$, was obtained from these data.

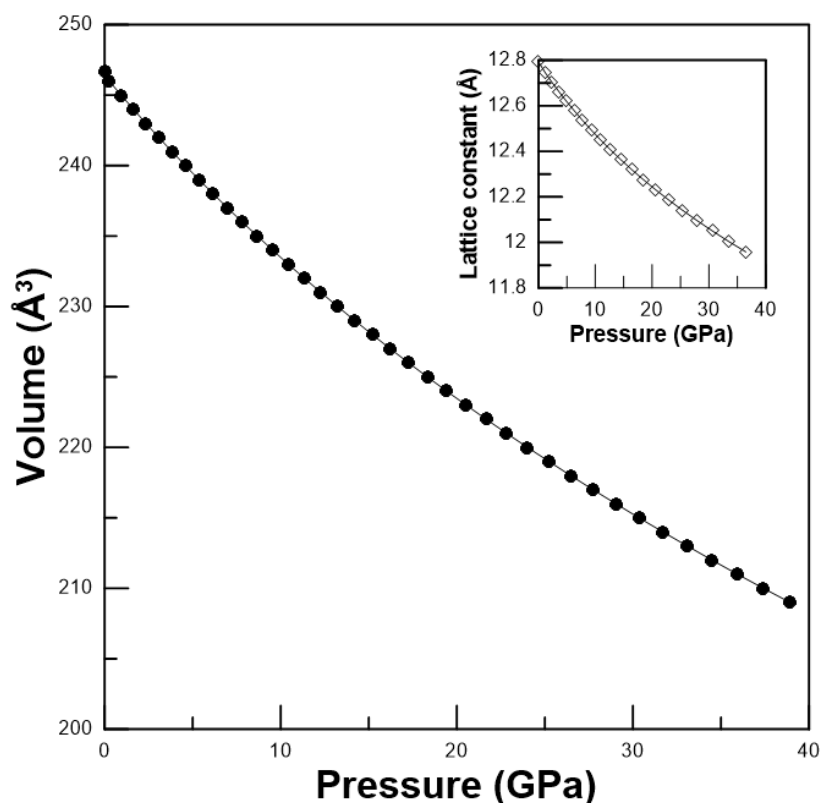


Figure 2. Pressure dependence of the volume. The inset shows the pressure dependence of the lattice constant.

The structural changes of $\text{Ca}_3\text{Y}_2\text{Ge}_3\text{O}_{12}$ under pressure are illustrated in Figures 3 and 4. The pressure dependence of the interatomic distances is shown in Figure 3. It can be observed that even at zero pressure, CaO_8 dodecahedra are slightly distorted with two different $\text{Ca}_{\text{dod}}\text{-O}$ distances (2.4587 and 2.5489 Å), while $\text{Y}_{\text{oct}}\text{-O}$ and $\text{Ge}_{\text{tet}}\text{-O}$ distances are 2.2327 and 1.7739 Å, respectively. When compared to distances in $\text{Sr}_3\text{Y}_2\text{Ge}_3\text{O}_{12}$, a garnet of the same family, the main difference is that $\text{Ca}_{\text{dod}}\text{-O}$ distances are slightly lower than $\text{Sr}_{\text{dod}}\text{-O}$ ones (5–3 %), while the $\text{Y}_{\text{oct}}\text{-O}$ and $\text{Ge}_{\text{tet}}\text{-O}$ distances are approximately the same in both compounds [21]. All the interatomic distances decrease with increasing pressure. However, whereas $\text{Y}_{\text{oct}}\text{-O}$ and $\text{Ge}_{\text{tet}}\text{-O}$ distances decrease at similar rates, -3.8×10^{-3} Å/GPa and -2.1×10^{-3} Å/GPa, respectively, one of the distances between Ca and O atoms varies more significantly than the other. The smaller distance ($\text{Ca}_{\text{dod}}\text{-O}$)2 changes at a rate of -4.95×10^{-3} Å/GPa, while the larger ($\text{Ca}_{\text{dod}}\text{-O}$)1 distance changes faster, at about -11.7×10^{-3} Å/GPa. Both become equal at around 15.9 GPa. This effect is common among garnets, e.g., the Lu-O distances become equal in $\text{Lu}_3\text{Ga}_5\text{O}_{12}$ [22] or the Y-O distances in $\text{Y}_3\text{Al}_5\text{O}_{12}$ [9].

The evolution with pressure of the polyhedral units of $\text{Ca}_3\text{Y}_2\text{Ge}_3\text{O}_{12}$ are plotted in Figure 4. The CaO_8 dodecahedra are the polyhedra with the major reduction in volume: 23.4% in the pressure range under study. In the case of the GeO_4 tetrahedra, the volume is almost constant along the pressure range with a small change of -0.09% . Finally, the YO_6 octahedra volume decreases by 13.9%.

The volume changes of the CaO_8 dodecahedra seem to be responsible for most of the volume reduction induced by pressure in $\text{Ca}_3\text{Y}_2\text{Ge}_3\text{O}_{12}$. In fact, the GeO_4 tetrahedra can be treated as rigid units within the structure.

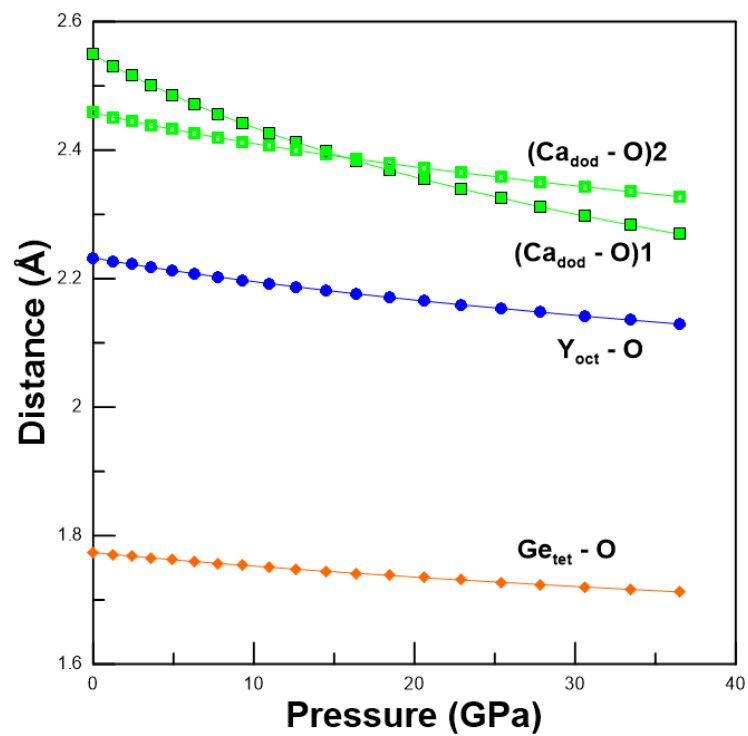


Figure 3. Evolution of interatomic distances as a function of pressure. Ca_{dod} stands for Ca atoms with dodecahedral coordination, Y_{oct} for Y atoms with octahedral coordination, and Ge_{tet} for Ge atoms with tetrahedral coordination.

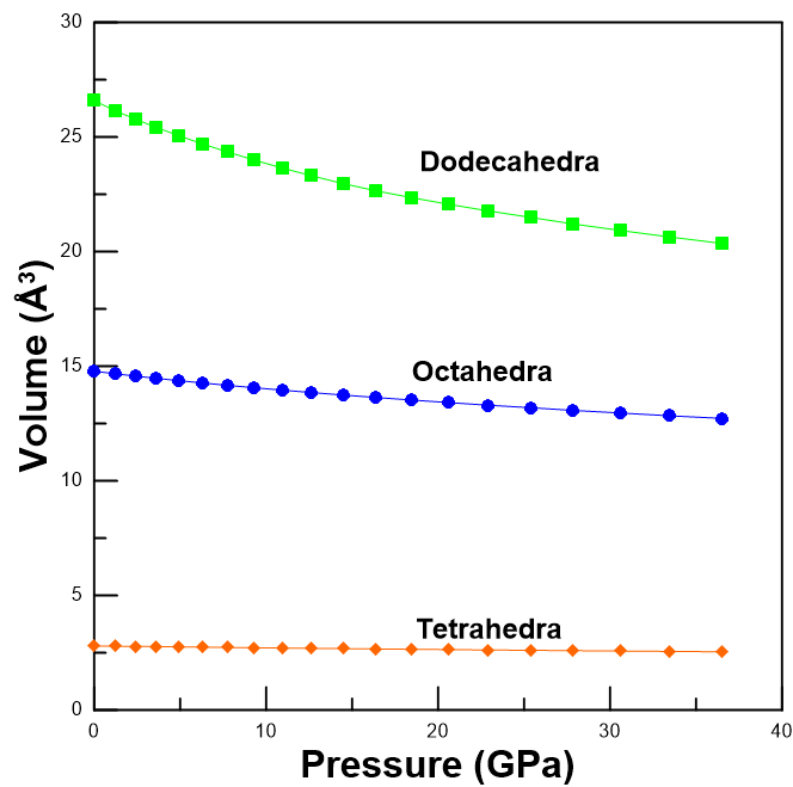


Figure 4. Pressure evolution of the polyhedral units: CaO₈ (green), YO₆ (blue), and GeO₄ (orange).

3.2. Electronic Structure

The electronic structure of $\text{Ca}_3\text{Y}_2\text{Ge}_3\text{O}_{12}$ has been scarcely investigated. Even though Baklanova et al. [23] have studied the electronic structure of this garnet at ambient pressure, the electronic properties under pressure are still unknown. Therefore, we performed band structure calculations at zero and different pressures of the $\text{Ca}_3\text{Y}_2\text{Ge}_3\text{O}_{12}$ garnet.

Figure 5 shows the electronic band structure at zero pressure. The valence band maxima and the conduction band minima are located at the Γ point, with a direct band gap of $E_g = 3.33$ eV. This value is in good agreement with the DFT result of 3.32 eV given in reference [23]. In the same reference, the experimental value obtained for the band gap is 5.56 eV, larger than the calculated value. As it is well known, the energy gap is underestimated by DFT compared with the experiments, although the order of magnitude of the pressure coefficients is in agreement.

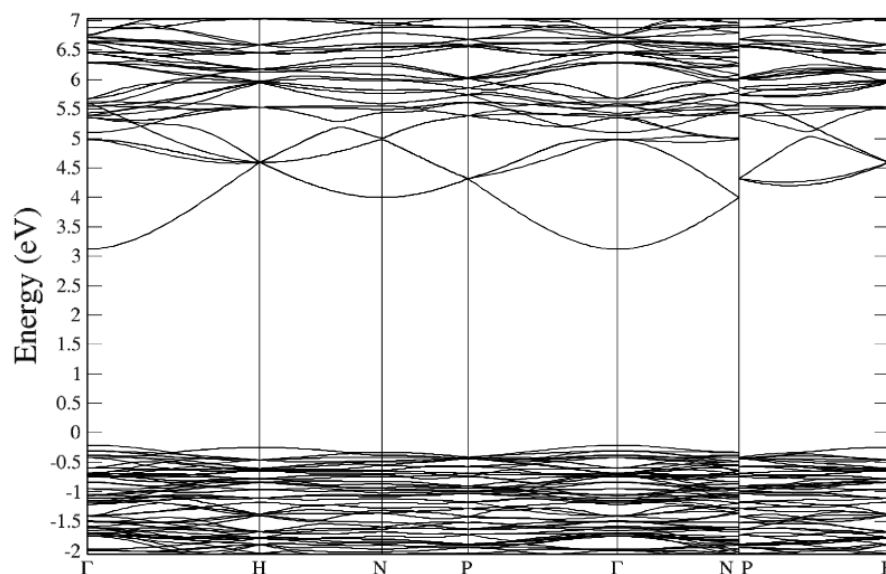


Figure 5. The band structure of $\text{Ca}_3\text{Y}_2\text{Ge}_3\text{O}_{12}$ along high symmetry directions in the Brillouin zone, at zero pressure.

As observed, the dispersion of the upper valence bands, VB, is small, similar to other garnets [9,22]. On the other hand, at the Γ point, the band at the bottom of the conduction bands, CB, is well separated with respect to the other conduction bands. To understand the nature of the electronic structure of $\text{Ca}_3\text{Y}_2\text{Ge}_3\text{O}_{12}$, we analyzed the total density of states (DOS) and the projected density of state (PDOS). The PDOS corresponding to the top of the VBs and bottom of CBs, from -2 to 7 eV (Figure 6), agrees with previous results [23]. O-2p states dominate the top of the valence bands. The bottom of the CBs is dominated by Y-4d states, with a contribution of O-2p states and a minor contribution of O-2s states near 5.5 eV.

As stated above, although the DFT calculations underestimate the band gap energy, they provide a good description of the pressure dependence of the band gap. To study the effect of pressure on electronic properties, we obtained the band structure of this compound under pressure. According to our calculations, the band gap remains direct in all the stability ranges and increases with a pressure derivative of 29.5 meV/GPa (Figure 7).

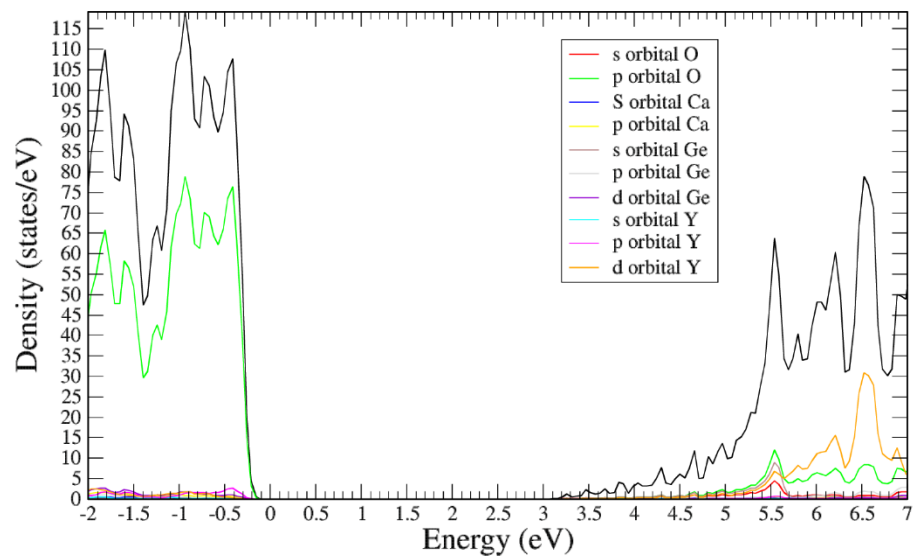


Figure 6. The total (DOS) and partial (PDOS) density of states of $\text{Ca}_3\text{Y}_2\text{Ge}_3\text{O}_{12}$, at zero pressure. The black curve represents the DOS.

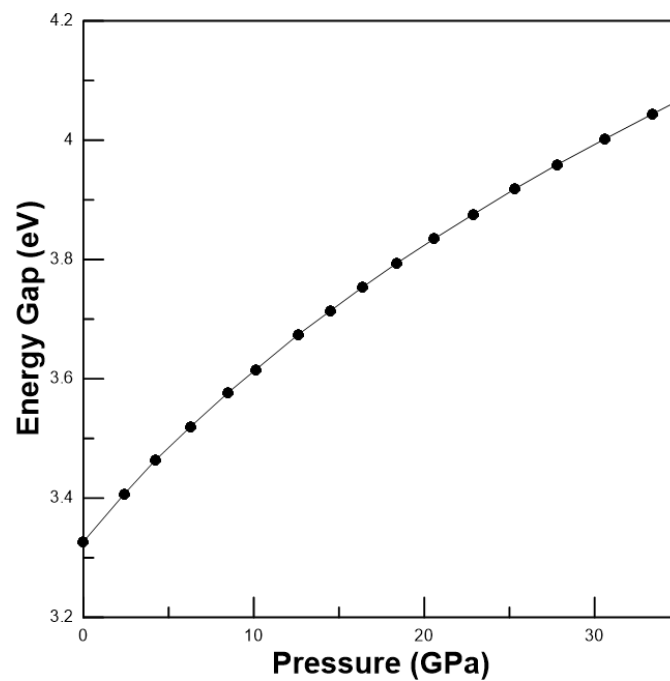


Figure 7. The pressure dependence of the band gap energy of $\text{Ca}_3\text{Y}_2\text{Ge}_3\text{O}_{12}$.

3.3. Elastic Properties

Since $\text{Ca}_3\text{Y}_2\text{Ge}_3\text{O}_{12}$ has a cubic structure, it has, therefore, only three independent elastic constants: C_{11} , C_{12} , and C_{44} . The elastic constants allow us to obtain the elastic moduli, bulk modulus (B), shear modulus (G), Young's modulus, and Poisson's ratio (ν) that describe the significant elastic properties of a compound along with the B/G ratio.

Cubic crystals the bulk modulus, B , are defined as the following:

$$B = \frac{C_{11} + 2C_{12}}{3}$$

The shear modulus in the scheme of Hill [24], G_H , can be expressed as the average between the upper bond, in the scheme of Voigt, G_V , and the lower bond, in scheme of Reuss, G_R , [25,26]. In the present case [8,27]:

$$G_H = \frac{1}{2} \left[\frac{C_{11} - C_{12} + 3C_{44}}{5} + \frac{5C_{44}(C_{11} - C_{12})}{4C_{44} + 3(C_{11} - C_{12})} \right]$$

The Young's modulus and the Poisson's ratio can be defined as the following:

$$E_x = \frac{9B_x G_x}{3B_x + G_x}$$

and

$$\nu_x = \frac{E_x - 2G_x}{2G_x}$$

where the subscript x refers to the symbols V, R, and H.

The computed elastic constants, C_{ij} , and the elastic moduli at 0 GPa are presented in Tables 2 and 3. The bulk modulus, the inverse of the compressibility, is related to the material resistance to hydrostatic pressure. The bulk modulus computed through the elastic constants, 112.430 GPa, is in excellent agreement with the value obtained with the EOS using total energy calculations, 111.24 GPa. This is an indication of the quality and consistency of our simulations. The Young modulus, 129.94 GPa, provides a measure of the material stiffness. Young's modulus, Poisson's ratio, and the B/G ratio are essential for engineering applications. B/G is 2.26; therefore, according to the Pugh criterion ($B/G > 1.75$), $\text{Ca}_3\text{Y}_2\text{Ge}_3\text{O}_{12}$ behaves like a ductile material at 0 GPa [28]. The Poisson's ratio is $\nu = 0.31$; hence, the ionic bonding is predominant against the covalent bonding, and the interatomic forces can still be considered predominantly central [29,30].

Table 2. Elastic constants in GPa of $\text{Ca}_3\text{Y}_2\text{Ge}_3\text{O}_{12}$ at 0 GPa.

C_{11}	C_{12}	C_{44}
199.43	68.93	41.38

Table 3. Elastic moduli B, E, and G, the B/G and the Poisson's ratio, ν , in the Voigt, Reuss, and Hill approximations, at 0 GPa.

	Voigt	Reuss	Hill
Bulk modulus (GPa)	112.4	112.43	112.43
Shear modulus (GPa)	50.93	48.47	49.70
Young modulus (GPa)	132.74	127.14	129.94
Poisson's ratio	0.30	0.31	0.31
Bulk/shear ratio	2.21	2.32	2.26

This compound is stable at zero pressure; hence, the elastic constants fulfill the Born stability criteria [31]:

$$C_{11} - C_{12} > 0, C_{11} + 2C_{12} > 0, \text{ and } C_{44} > 0$$

However, when hydrostatic pressure is applied to the crystal, the above criteria to describe the stability limits of a cubic crystal are not adequate. Moreover, the relevant magnitudes that describe the elastic properties are the elastic stiffness coefficients, B_{ij} , related to the elastic constants through the following relationships [32,33]:

$$B_{11} = C_{11} - P, B_{12} = C_{12} + P, \text{ and } B_{44} = C_{44} - P$$

The evolution of the B_{ij} with pressure is plotted in Figure 8. The diagonal coefficient B_{11} and the B_{12} coefficient increase with pressure in the studied pressure range. However, the diagonal coefficient B_{44} decreases rapidly, becoming negative at about 45 GPa. B_{11} is higher than B_{44} ; this indicates that the resistance to a shear deformation is weaker than the resistance to compression.

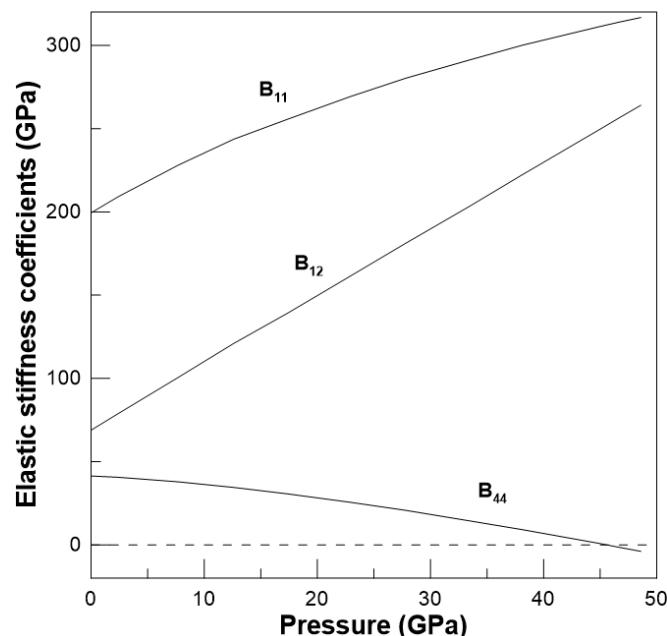


Figure 8. Pressure evolution of the elastic stiffness coefficients, B_{ij} .

The elastic stiffness coefficients enable us to study the evolution of the elastic properties under pressure. Replacing the C_{ij} elastic constants with the B_{ij} elastic stiffness coefficients in the above expressions, we obtain the analytical expressions for the elastic moduli, valid under pressure [31,34]. The pressure dependence of the elastic moduli with pressure up to 50 GPa is displayed in Figure 9. The bulk modulus increases almost linearly with increasing pressure. Both the shear modulus and the Young modulus decrease, and their values converge at high pressure. The Poisson's ratio becomes larger, and this can be interpreted as an increase in metallization. The B/G ratio indicates that the material is ductile until approximately 45 GPa; above this pressure, there is a dramatic change in the slope (Figure 10a). This could indicate a possible mechanical instability at higher pressures.

To study the mechanical stability of a crystal under pressure, the generalized Born stability criteria must be employed [31,35]. In the present case, as stated above, these criteria can be written as the following:

$$M_1 = B_{11} - B_{12} > 0, \quad M_2 = B_{11} + 2B_{12} > 0, \quad M_3 = B_{44} > 0 \quad (1)$$

These generalized stability criteria are plotted as a function of pressure in Figure 10b. The M_3 stability criterion is violated at 45.7 GPa. This result indicates that the $\text{Ca}_3\text{Y}_2\text{Ge}_3\text{O}_{12}$ garnet is mechanically unstable above this pressure. Experimental studies on garnets report that an amorphous phase appears at high pressure [8,22,36]. However, in the present case, as we will see in the next section, the $\text{Ca}_3\text{Y}_2\text{Ge}_3\text{O}_{12}$ garnet becomes dynamically unstable at pressure over 34.4 GPa.

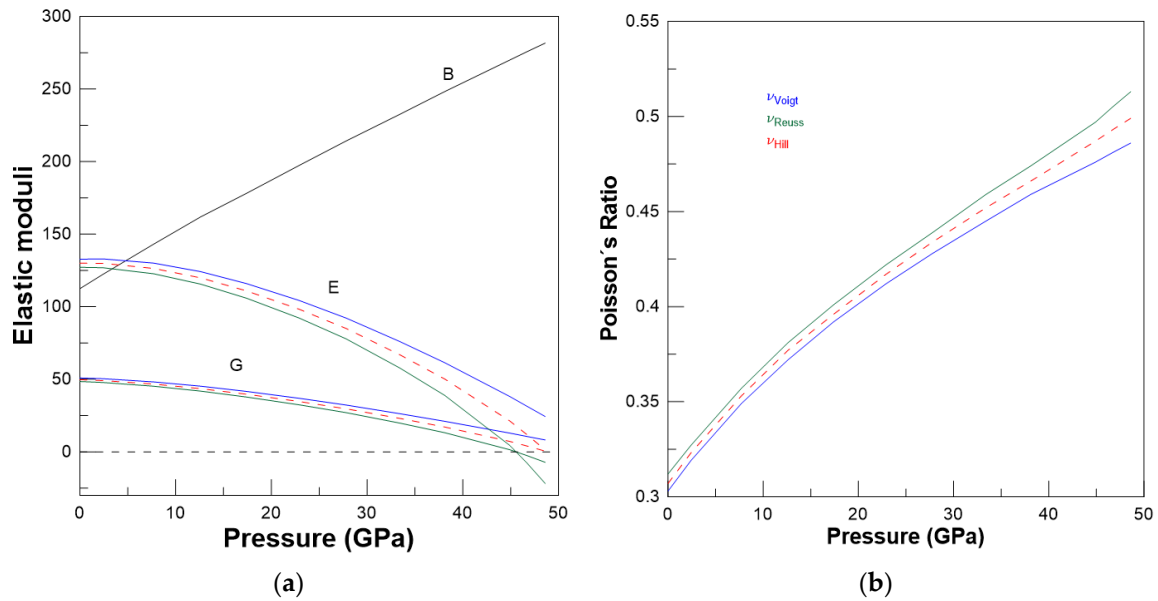


Figure 9. (a) Pressure evolution of the elastic moduli: bulk modulus, B, Young Modulus, E, and shear modulus, G. The blue line represents the moduli in the Voigt approximation, the green line in the Reuss approximation, and the red one in the Hill approximation. (b) Pressure evolution of the Poisson's ratio in the three approximations: Voigt, Reuss, and Hill.

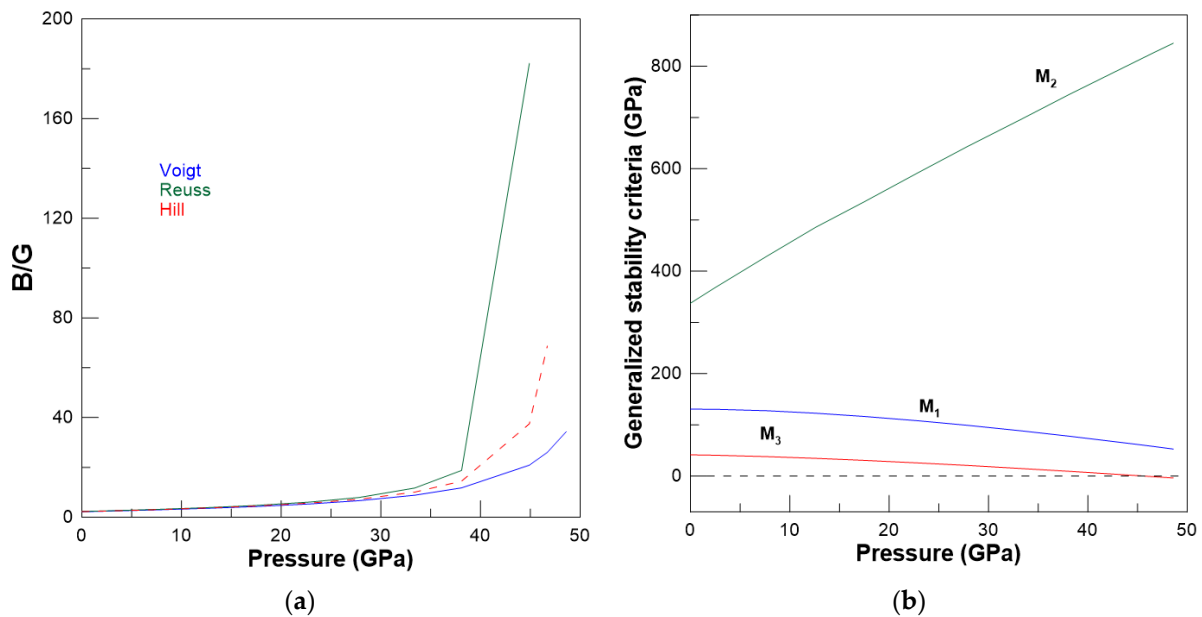


Figure 10. (a) Pressure evolution of the B/G ratio in the approximations of Voigt, Reuss, and Hill. (b) Generalized stability criteria as a function of pressure.

3.4. Vibrational Properties

The $\text{Ca}_3\text{Y}_2\text{Ge}_3\text{O}_{12}$ garnet belongs to the $Ia-3d$ space group and, according to group theory, has 98 vibrational modes. At the zone center, they can be classified as 25 Raman active modes ($3A_{1g} + 8E_g + 14T_{2g}$), 17 infrared active modes ($17T_{1u}$), and 55 silent modes ($16T_{2u} + 14T_{1g} + 5A_{2u} + 5A_{2g} + 10E_u + 5A_{1u}$), which are optically inactive.

Figure 11 shows the phonon dispersion. It can be observed that the phonon spectrum could be divided into three regions. The low-frequency region ranges up to approximately 400 cm^{-1} and is separated by a small gap from the medium-frequency region, which is

very narrow and reaches up to 510 cm^{-1} . The high-frequency region extends from 625 to 780 cm^{-1} .

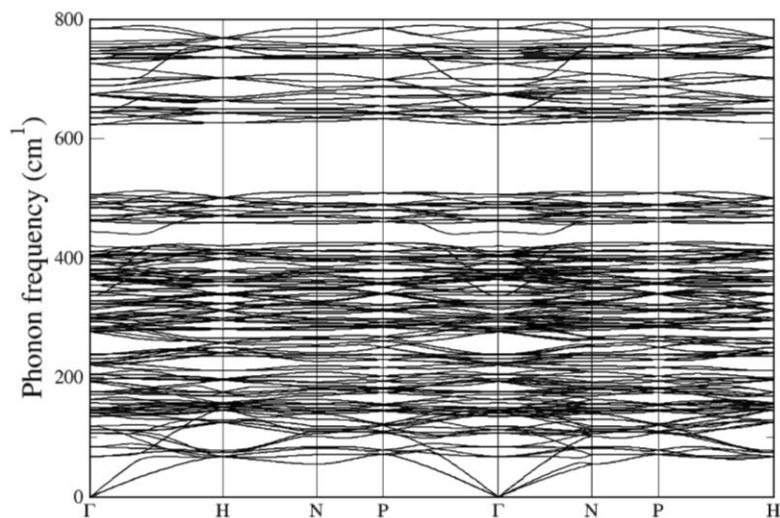


Figure 11. Phonon dispersion of $\text{Ca}_3\text{Y}_2\text{Ge}_3\text{O}_{12}$ garnet at 0 GPa along the high symmetry directions.

The Raman modes are connected with the vibration of the different polyhedral units strongly coupled to each other; therefore, the attribution of each mode to a single unit is not straightforward. To analyze the dynamical contribution of each atom, the total phonon density of states (DOS) and the partial density of states (PDOS) were calculated (see Figure 12). As shown, in the case of $\text{Ca}_3\text{Y}_2\text{Ge}_3\text{O}_{12}$, the PDOS is very compact at low and medium frequencies, between 100 and 510 cm^{-1} , and also in the high-frequency region between 625 and 780 cm^{-1} . The contributions of Y atoms are located at the low- and medium-frequency regions, mainly up to 200 cm^{-1} . Ca atoms also contribute in these regions, although the contribution is small in the region of very low frequencies. Ge atoms have a small contribution in the region from 200 to 500 cm^{-1} and a larger one in the high-frequency region. Finally, the O atoms have more significant contributions, spread over all frequencies, mainly in the high-frequency region.

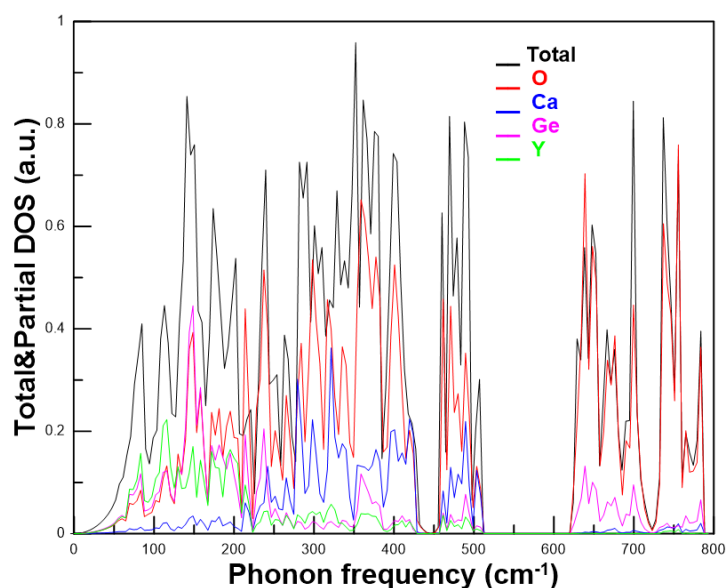


Figure 12. Total and partial phonon density of states at zero pressure. The black line represents the total DOS, and the contributions of O, Ca, Ge, and Y atoms are represented by the red, blue, magenta, and green lines, respectively.

The pressure dependence of the calculated frequencies has been fitted with a second-order polynomial. All theoretical Raman active modes are reported at zero pressure in Table 4, along with the pressure derivative coefficients, $d\omega/dP$, and the Grüneisen parameters, $\gamma = (d\omega/dP)/(B_0/\omega_0)$, where B_0 is the bulk modulus and ω_0 the frequency of the corresponding mode at zero pressure.

Table 4. Wavenumbers of Raman active vibrational frequencies at zero pressure, ω_0 , their pressure coefficients, $d\omega/dP$, and Grüneisen parameters, γ , of $\text{Ca}_3\text{Y}_2\text{Ge}_3\text{O}_{12}$ garnet.

Mode Symmetry	ω_0 (cm^{-1})	$d\omega/dP$ ($\text{cm}^{-1}/\text{GPa}$)	γ
E_g	141.47	0.958	0.75
T_{2g}	142.84	1.539	1.20
T_{2g}	152.62	2.190	1.59
T_{2g}	194.70	1.430	0.82
T_{2g}	234.25	2.320	1.10
T_{2g}	295.08	3.626	1.37
E_g	301.61	2.169	0.80
T_{2g}	306.04	5.405	1.96
E_g	304.89	3.666	1.34
A_{1g}	325.85	3.768	1.28
T_{2g}	354.64	3.495	1.10
T_{2g}	350.29	6.711	2.13
E_g	380.55	3.140	0.92
E_g	400.63	5.960	1.65
T_{2g}	408.54	3.975	1.08
A_{1g}	444.83	4.085	1.02
T_{2g}	466.97	4.222	1.00
E_g	485.32	3.118	0.71
T_{2g}	483.25	3.839	0.88
T_{2g}	655.21	4.998	0.85
T_{2g}	676.95	4.594	0.75
E_g	701.16	4.755	0.76
E_g	736.78	4.354	0.66
A_{1g}	759.40	4.295	0.63
T_{2g}	786.11	4.062	0.57

The evolution of the Raman modes of this garnet with pressure is presented in Figure 13. Most modes harden under compression; however, the frequencies of the lowest Raman modes change slightly. The modes on the low- and medium-frequency regions are related to movements of Ca, Ge, Y, and O atoms and exhibit very different pressure coefficients, since they involve several types of bonds with diverse compressibility. Due to the significant differences between the pressure dependence of these modes, crossing and anti-crossing phenomena are observed in the medium-frequency region. The highest modes, however, increase with pressure with similar coefficients and exhibit similar and low Grüneisen parameters.

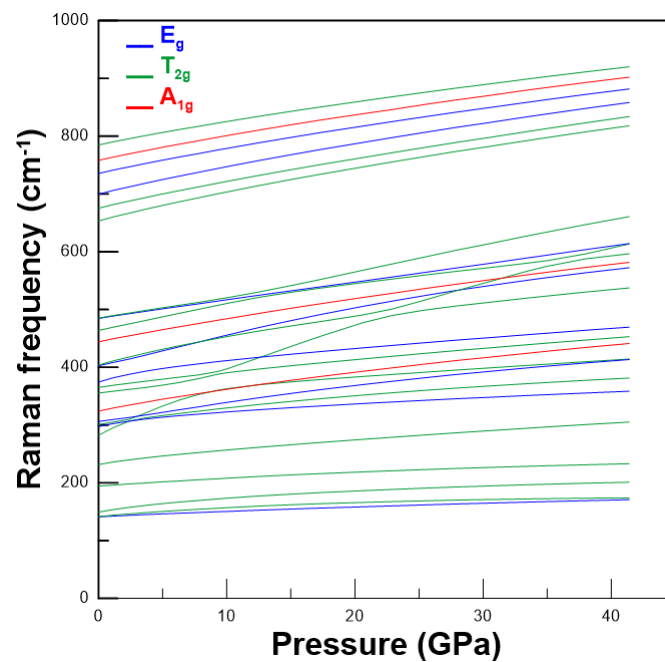


Figure 13. Theoretical evolution with pressure of Raman modes of the $\text{Ca}_3\text{Y}_2\text{Ge}_3\text{O}_{12}$ garnet.

Additionally, the pressure evolution of the infrared modes is plotted in Figure 14. As in the case of Raman modes, there is clearly a large gap between the medium- and high-frequency region. The phonons in the medium- and high-frequency regions harden under pressure, and there are several anti-crossing phonons in the medium region. Except for the lowest mode ($\omega_0 = 67.96 \text{ cm}^{-1}$), all the phonons in the low-frequency region are very slightly affected by pressure. The frequency values, pressure derivative, and Grüneisen parameters for the infrared modes are reported in Table 5.

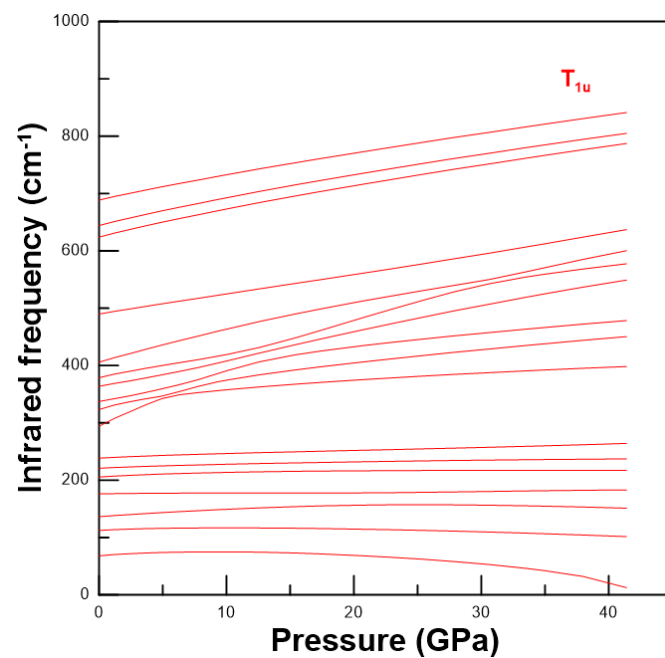
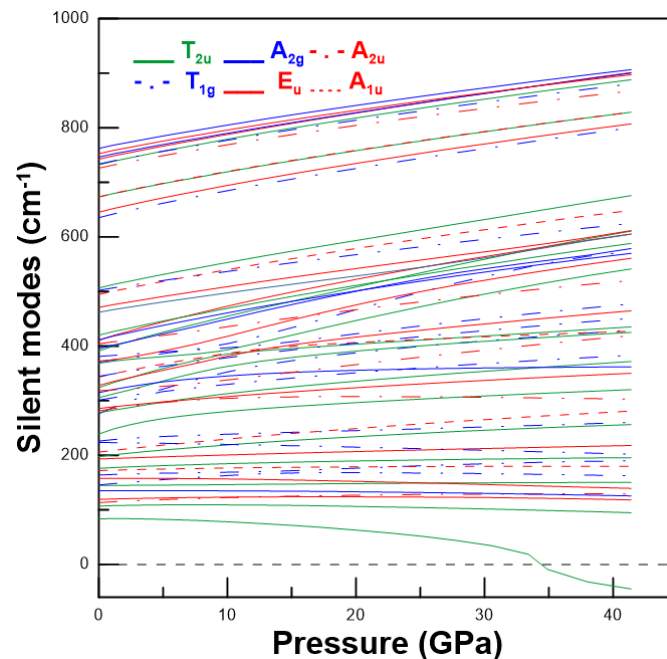


Figure 14. Theoretical evolution with the pressure of infrared modes of the $\text{Ca}_3\text{Y}_2\text{Ge}_3\text{O}_{12}$ garnet.

Table 5. Infrared active vibrational modes, ω_0 , pressure coefficients, $d\omega/dP$, and Grüneisen parameters, γ , of $\text{Ca}_3\text{Y}_2\text{Ge}_3\text{O}_{12}$ garnet.

Mode Symmetry	ω_0 (cm^{-1})	$d\omega/dP$ ($\text{cm}^{-1}/\text{GPa}$)	γ
T _{1u}	67.96	1.418	2.32
T _{1u}	113.97	0.397	0.39
T _{1u}	136.53	1.566	1.27
T _{1u}	176.95	−0.017	−0.01
T _{1u}	207.04	0.706	0.38
T _{1u}	221.62	0.661	0.33
T _{1u}	239.60	0.656	0.30
T _{1u}	311.77	4.571	1.63
T _{1u}	326.13	4.881	1.66
T _{1u}	333.97	6.179	2.06
T _{1u}	359.84	5.185	1.60
T _{1u}	372.30	5.558	1.66
T _{1u}	409.26	5.375	1.46
T _{1u}	490.98	3.269	0.74
T _{1u}	625.86	4.871	0.865
T _{1u}	645.88	3.118	0.71
T _{1u}	690.02	4.383	0.70

Finally, the pressure evolution of the 55 silent modes is presented in Figure 15. The most crucial point is the softening of the lower silent mode (T_{2u}).

**Figure 15.** Theoretical evolution with the pressure of silent modes of $\text{Ca}_3\text{Y}_2\text{Ge}_3\text{O}_{12}$ garnet.

At 34.4 Gpa, this T_{2u} mode becomes imaginary, as shown in Figure 16. It is important to note that this indicates a dynamical instability at 34.4 GPa. Therefore, our results evidence that, under hydrostatic pressure, this compound becomes dynamically unstable.

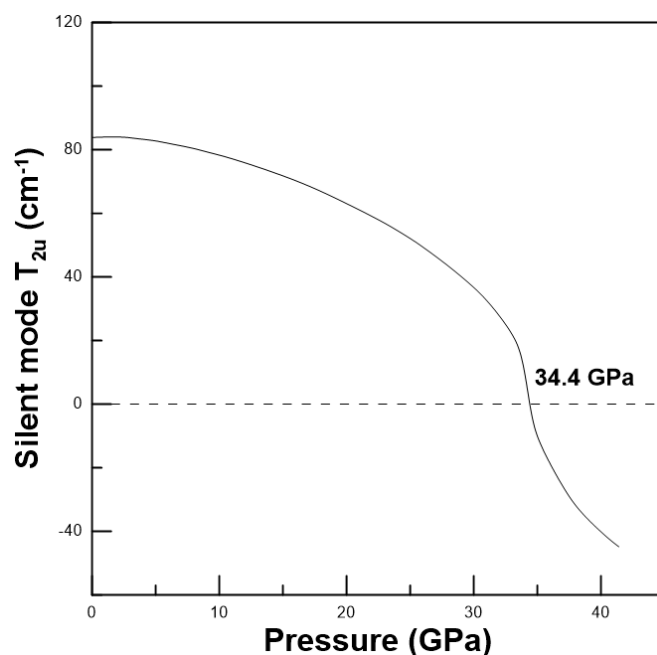


Figure 16. Theoretical evolution with pressure of silent mode T_{2u} of the $\text{Ca}_3\text{Y}_2\text{Ge}_3\text{O}_{12}$ garnet.

We analyzed this soft phonon and obtained a triclinic $P-1$ structure with 80 atoms in the cell at positions $1a$ ($x y z$). By studying the stability of this new structure, we obtained that it is also dynamically unstable, so we discard it as a possible high-pressure phase of this garnet.

4. Conclusions

An ab initio study of the structural, electronic, elastic, and vibrational properties of the $\text{Ca}_3\text{Y}_2\text{Ge}_3\text{O}_{12}$ garnet was performed both at ambient and under hydrostatic pressure.

The lattice parameter compares nicely with the experimental value at 0 GPa. The evolution of the lattice parameter and interatomic distances under compression, the equation of state, and the compressibility are reported. The dodecahedral units (CaO_8 in the present case) that account for most of the volume changes are distorted and behave under pressure in a common way among garnets.

The electronic band structure agrees with previous theoretical data and shows a direct band gap at Γ that increases with increasing pressure.

The elastic constants and elastic stiffness coefficients were accurately determined and the elastic behavior of the $\text{Ca}_3\text{Y}_2\text{Ge}_3\text{O}_{12}$ garnet was analyzed. The pressure evolution of B , G , and E elastic moduli and the Poisson's ratio were reported. The B/G relation indicates that the material is ductile in the whole pressure stability range and more sensitive to volume compression than to shear deformation ($B > G$). The study of the stability criteria indicates that the garnet is mechanically unstable above 45.7 GPa.

The total and partial phonon density of states were analyzed to determine each atom's contribution to the different vibrational modes. The pressure evolutions of the Raman, infrared, and silent modes were presented. At 34.4 GPa, the lower silent mode (T_{2u}) softens and becomes imaginary; this means that the garnet structure is unstable at a pressure above 34.4 GPa.

Author Contributions: Both authors contributed equally to this work: simulations, analysis and interpretation of results, and manuscript writing, A.M., P.R.-H. All authors have read and agreed to the published version of the manuscript.

Funding: This research was funded by the Spanish Research Agency (AEI) and the Spanish Ministry of Science and Investigation (MCIN) under grant PID2019-106383GB-43 (DOI: 10.13039/501100011033) and RED2018-102612-T (MALTA Consolider-Team Network).

Data Availability Statement: All relevant data that support the findings of this study are available from the corresponding authors upon request.

Acknowledgments: The authors thank the financial support from the Spanish Research Agency (AEI) and Spanish Ministry of Science and Investigation (MCIN) under grant PID2019-106383GB-43 (DOI: 10.13039/501100011033) and RED2018-102612-T (MALTA Consolider-Team Network).

Conflicts of Interest: The authors declare no conflict of interest.

References

1. Karato, S.-I.; Wang, Z.; Liu, B.; Fujino, K. Plastic deformation of garnets: Systematics and implications for the rheology of the mantle transition zone. *Earth Planet. Sci. Lett.* **1995**, *130*, 13–30. [[CrossRef](#)]
2. Speghini, A.; Piccinelli, F.; Bettinelli, M. Synthesis, characterization and luminescence spectroscopy of oxide nanopowders activated with trivalent lanthanide ions: The garnet family. *Opt. Mater.* **2011**, *33*, 247–257. [[CrossRef](#)]
3. Rodríguez-Mendoza, U.R.; León-Luis, S.F.; Muñoz-Santiuste, J.E.; Jaque, D.; Lavín, V. Nd³⁺-doped Ca₃Ga₂Ge₃O₁₂ garnet: A new optical pressure sensor. *J. Appl. Phys.* **2013**, *113*, 213517. [[CrossRef](#)]
4. León-Luis, S.F.; Muñoz-Santiuste, J.E.; Lavín, V.; Rodríguez-Mendoza, U. Optical pressure and temperature sensor based on the luminescence properties of Nd³⁺ ion in a gadolinium scandium gallium garnet crystal. *Opt. Express* **2012**, *20*, 10393–10398. [[CrossRef](#)]
5. Nishiura, S.; Tanabe, A.; Fujioka, F.Y. Properties of transparent Ce:YAG ceramic phosphors for white LED. *Opt. Mater.* **2011**, *33*, 688–691. [[CrossRef](#)]
6. Cui, J.; Zheng, Y.; Wang, Z.; Cao, L.; Wang, X.; Yao, Y.; Zhang, M.; Zheng, M.; Yang, Z.; Li, P. Improving the luminescence thermal stability of Ca₃Y₂Ge₃O₁₂: Cr³⁺ based on cation substitution and its application in NIR LEDs. *Mater. Adv.* **2022**, *3*, 2772–2778. [[CrossRef](#)]
7. Mao, N.; Liu, S.; Song, Z.; Yu, Y.; Liu, Q. A broadband near-infrared phosphor Ca₃Y₂Ge₃O₁₂:Cr³⁺ with garnet structure. *J. Alloys Compd.* **2021**, *863*, 158699. [[CrossRef](#)]
8. Monteseuro, V.; Rodríguez-Hernández, P.; Lavín, V.; Manjón, F.J.; Muñoz, A. Electronic and elastic properties of Yttrium gallium garnet under pressure from ab initio studies. *J. Appl. Phys.* **2013**, *113*, 183505. [[CrossRef](#)]
9. Monteseuro, V.; Rodríguez-Hernández, P.; Muñoz, A. Yttrium aluminum garnet under pressure: Structural, elastic, and vibrational properties from ab initio studies. *J. Appl. Phys.* **2015**, *118*, 245902. [[CrossRef](#)]
10. Mookherjee, M. High-pressure elasticity of sodium majorite garnet, Na₂MgSi₅O₁₂. *Am. Mineralogist.* **2014**, *99*, 2416–2423. [[CrossRef](#)]
11. Kresse, G.; Furthmüller, J. Efficient iterative schemes for ab initio total-energy calculations using a plane-wave basis set. *Phys. Rev. B* **1996**, *54*, 11169–11186. [[CrossRef](#)] [[PubMed](#)]
12. Kresse, G.; Furthmüller, J. Efficiency of ab-initio total energy calculations for metals and semiconductors using a plane-wave basis set. *Comput. Mater. Sci.* **1996**, *6*, 15–50. [[CrossRef](#)]
13. Blöchl, P.E. Projector augmented-wave method. *Phys. Rev. B* **1994**, *50*, 17953–17979. [[CrossRef](#)] [[PubMed](#)]
14. Perdew, J.P.; Ruzsinszky, A.; Csonka, G.I.; Vydrov, O.A.; Scuseria, G.E.; Constantin, L.A.; Zhou, X.; Burke, K. Restoring the Density-Gradient Expansion for Exchange in Solids and Surfaces. *Phys. Rev. Lett.* **2008**, *100*, 136406. [[CrossRef](#)]
15. Monkhorst, H.J.; Pack, J.D. Special points for Brillouin-zone integrations. *Phys. Rev. B* **1976**, *13*, 5188–5192. [[CrossRef](#)]
16. Togo, A.; Tanaka, I. First principles phonon calculations in materials science. *Scr. Mater.* **2015**, *108*, 1–5. [[CrossRef](#)]
17. Le Page, Y.; Saxe, P. Symmetry-General Least-Squares Extraction of Elastic Data for Strained Materials from Ab Initio Calculations of Stress. *Phys. Rev. B* **2002**, *65*, 104104. [[CrossRef](#)]
18. Levy, D.; Barbier, J. Normal and inverse garnets: Ca₃Fe₂Ge₃O₁₂, Ca₃Y₂Ge₃O₁₂ and Mg₃Y₂Ge₃O₁₂. *Acta Cryst.* **1999**, *55*, 1611–1614. [[CrossRef](#)]
19. Birch, F. Finite Elastic Strain of Cubic Crystals. *Phys. Rev.* **1947**, *71*, 809–824. [[CrossRef](#)]
20. Milman, V.; Nobes, R.H.; Akhmatkaya, E.V.; Winkler, B.; Pickard, C.J.; White, J.A. Ab initio study of the structure and compressibility of garnets. In *Properties of Complex Inorganic Solids*; Meike, A., Gonis, A., Turchi, P.E.A., Rajan, K., Eds.; Kluwer Academic/Plenum: New York, NY, USA, 2000; Volume 3, pp. 417–427.
21. Marin, S.J.; O’Keeffe, M.; Young, V.G., Jr.; Von Dreele, R.B. The crystal structure of Sr₃Y₂Ge₃O₁₂. *J. Solid State Chem.* **1991**, *91*, 173–175. [[CrossRef](#)]
22. Monteseuro, V.; Rodríguez-Hernández, P.; Ortiz, H.M.; Venkatramu, V.; Manjón, F.J.; Jayasankar, C.K.; Lavín, V.; Muñoz, A. Structural, elastic and vibrational properties of nanocrystalline lutetium gallium garnet under high pressure. *Phys. Chem. Chem. Phys.* **2015**, *17*, 9454–9464. [[CrossRef](#)] [[PubMed](#)]
23. Baklanova, Y.V.; Enyashin, A.N.; Maksimova, L.G.; Tyutyunnik, A.P.; Chufarov, A.Y.; Gorbatov, E.V.; Baklanova, I.V.; Zubkov, V.G. Sensitized IR luminescence in Ca₃Y₂Ge₃O₁₂: Nd³⁺, Ho³⁺ under 808 nm laser excitation. *Ceram. Int.* **2018**, *44*, 6959–6967. [[CrossRef](#)]
24. Hill, R. The Elastic Behaviour of a Crystalline Aggregate. *Proc. Phys. Soc. Sect. A* **1952**, *65*, 349. [[CrossRef](#)]
25. Voigt, W. *Lehrbuch der Kristallphysik (Mit Ausschluss der Kristalloptik)*; B.G. Teubner: Leipzig/Berlin, Germany, 1928.

26. Reuss, A. Berechnung der Fließgrenze von Mischkristallen auf Grund der Plastizitätsbedingung für Einkristalle. *J. Appl. Math. Mech.* **1929**, *9*, 49–58. [[CrossRef](#)]
27. Erba, A.; Mahmoud, A.; Orlando, R.; Dovesi, R. Elastic properties of six silicate garnet end members from accurate ab initio simulations. *Phys. Chem. Miner.* **2014**, *41*, 151–160. [[CrossRef](#)]
28. Pugh, S.F. XCII. Relations between the elastic moduli and the plastic properties of polycrystalline pure metals. *Lond. Edinb. Dublin Philos. Mag. J. Sci.* **1954**, *45*, 823–843. [[CrossRef](#)]
29. Brazhkin, V.V.; Lyapin, A.G.; Hemley, R.J. Harder than diamond: Dreams and reality. *Philos. Mag. A* **2002**, *82*, 231–253. [[CrossRef](#)]
30. Greaves, G.N.; Greer, A.L.; Lakes, R.S.; Rouxel, T. Poisson's ratio and modern materials. *Nat. Mater.* **2011**, *10*, 823–837. [[CrossRef](#)]
31. Born, M.; Huang, K. *Dynamical Theory of Crystal Lattices*; Clarendon Press: London, UK, 1954.
32. Wallace, D.C. *Thermodynamics of Crystals*; Dover Publications: New York, NY, USA, 1998.
33. Grimvall, G.; Magyar-Köpe, B.; Ozolins, V.; Persson, K.A. Lattice instabilities in metallic elements. *Rev. Mod. Phys.* **2012**, *84*, 945–986. [[CrossRef](#)]
34. Wallace, D.C. Thermoelasticity of Stressed Materials and Comparison of Various Elastic Constants. *Phys. Rev.* **1967**, *162*, 776–789. [[CrossRef](#)]
35. Wang, J.; Yip, S.; Phillpot, S.R.; Wolf, D. Crystal instabilities at finite strain. *Phys. Rev. Lett.* **1993**, *71*, 4182–4185. [[CrossRef](#)] [[PubMed](#)]
36. Hua, H.; Mirov, S.; Vohra, Y.K. High-pressure and high-temperature studies on oxide garnets. *Phys. Rev. B* **1996**, *54*, 6200–6209. [[CrossRef](#)] [[PubMed](#)]

Disclaimer/Publisher's Note: The statements, opinions and data contained in all publications are solely those of the individual author(s) and contributor(s) and not of MDPI and/or the editor(s). MDPI and/or the editor(s) disclaim responsibility for any injury to people or property resulting from any ideas, methods, instructions or products referred to in the content.